STM JOURNALS

Journal of
Polymer & Composites

ISSN: 2321-2810 (Online)
ISSN: 2321-8525 (Print)
Volume 14, Special Issue 2, 2026
DOI (Journal): 10.37591/JoPC

https://journals.stmjournals.com/jopc

Research JoPC

Polymer Waste-Derived Activated Carbon from PET for High-Efficiency Supercapacitor Electrodes

Baburao Gaddala[1,*], Srinivas Ganganagunta[2], Abha Gupta[3], Gautam Prasad Dewangan[4], Jeyadevan S.[5]

Abstract

The exponential increase in plastic waste, particularly Polyethylene Terephthalate (PET)—a polymer characterized by its repeating aromatic terephthalate units and ester linkages—has escalated into a global environmental crisis. This study details a low-cost synthesis of porous carbon materials derived from waste PET via pyrolysis followed by chemical activation with calcium hydroxide ($Ca(OH)_2$). During pyrolysis, the PET polymer chains undergo thermal degradation, where the aromatic rings in the backbone serve as precursors for a stable carbon framework. The resulting activated carbon was evaluated as an electrode for supercapacitor applications. FTIR spectroscopy revealed a significant reduction in oxygen-containing functional groups (such as C=O and C-O bonds inherent in the original polyester), indicating successful carbonization. XRD and Raman analyses confirmed an amorphous structure with localized graphitic domains, essential for electrical conductivity. SEM and TEM imaging showcased a highly interconnected, porous morphology, a stark contrast to the dense, non-porous nature of raw PET.BET analysis reported a high specific surface area of approximately 631 m^2/g. This developed pore architecture is critical for facilitating efficient ion diffusion and charge storage. The fabricated supercapacitor exhibited robust capacitive behavior, achieving a working voltage of 1.0 V and maintaining 38% voltage retention after 19.4 hours. A successful LED illumination test validated the device's ability to store and deliver power. This work demonstrates a circular economy approach, converting long-chain polymers into high-value energy materials to mitigate plastic pollution.

Keywords: Polymer waste, Polyethylene Terephthalate (PET), Activated carbon, Supercapacitor, Electrode material, Energy storage, Chemical activation

INTRODUCTION

Plastic materials have gradually replaced traditional materials like metal, wood, and glass because they are low-cost, flexible, easy to manufacture, and offer good performance in many applications. Among various plastics, Polyethylene Terephthalate (PET) is one of the most widely used thermoplastics, especially for packaging applications such as water bottles, soft drinks, food containers, and other consumer goods shown in Figure 1-Figure 2. The production and consumption of PET have grown rapidly over the years. Globally, PET production increased from 42 million tons in 2014 to about 72 million tons by 2020, reflecting its widespread industrial demand. In India alone, around 900 kilo-tons of PET was consumed during 2015-16, demonstrating its large-scale usage in the packaging sector. Furthermore, the consumption of PET bottles has increased drastically from 300 billion bottles in 2000 to 480 billion in 2016 and is expected to reach 583 billion bottles by 2021, indicating continuous growth in plastic waste generation [1].

***Author for Correspondence**
Baburao Gaddala

[1,4]Associate Professor, Department of Chemical Engineering, School of Studies of Engineering & Technology, Guru Ghasidas Vishwavidyalaya (A Central University), Bilaspur, Chhattisgarh, India
[2,3,5]Senior Lecturer, Department of Engineering &Technology, University of Technology and Applied Sciences-IBRA, North Al sharqia, Oman

Received Date: April 11, 2026
Accepted Date: April 20, 2026
Published Date: April 28, 2026

Citation: Baburao Gaddala, Srinivas Ganganagunta, Abha Gupta, Gautam Prasad Dewangan, Jeyadevan S. Polymer Waste-Derived Activated Carbon from PET for High-Efficiency Supercapacitor Electrodes. Polymer Composites. Journal of Polymer & Composites. 2026; 14(Special Issue 2): S1419–S1447p.


Figure 1. Waste PET bottles Figure 2 Small pieces of PET bottles

This rapid increase in PET consumption has led to the generation of huge amounts of plastic waste, making it a major environmental concern. Plastics are broadly classified into thermoplastics and thermosetting plastics. Thermoplastics, such as LDPE, HDPE, and PET, can be softened and reshaped upon heating, whereas thermosetting plastics, such as Bakelite and epoxy, become permanently hard and cannot be remolded [2]. PET belongs to the category of thermoplastics, specifically thermoplastic polyester, and is characterized by its aromatic structure, high strength, and thermal stability, which make it suitable for various industrial applications shown in Figure3. Despite its advantages, PET poses serious environmental and health risks due to its non-biodegradable nature. It accumulates in soil, water bodies, and oceans, leading to pollution, blockage of drainage systems, and harm to aquatic life. Over time, plastics degrade into microplastics, which can enter the food chain and cause potential health issues such as toxicity and hormonal imbalance. Additionally, improper disposal methods like burning release toxic gases, contributing to air pollution and respiratory problems. In recent years, there has been growing interest in converting plastic waste into valuable materials rather than treating it as waste [3]. PET is particularly suitable for such applications because it is carbon-rich and can be converted into porous carbon materials through pyrolysis. The concept of utilizing waste-derived polymers aligns with recent developments in sustainable composite materials, where industrial and agricultural wastes are incorporated as reinforcing phases to improve performance and reduce environmental impact [48–50]. The carbon obtained from PET exhibits high surface area, good electrical conductivity, and well-developed pore structure, which are essential properties for energy storage applications such as supercapacitors. Compared to other plastics, PET has a higher carbon yield and an aromatic structure that promotes the formation of stable and conductive carbon frameworks. Activation processes further enhance pore development, resulting in improved electrochemical performance. Conventional batteries, although widely used, suffer from several limitations such as slow charging, low power density, limited cycle life, and the use of toxic materials, which pose environmental concerns. Supercapacitors have emerged as an alternative energy storage device due to their fast charging capability, high power density, long cycle life, and better stability [4]. In this context, utilizing waste PET for the preparation of supercapacitor electrode materials offers a dual advantage: it provides a low-cost, sustainable source of high-performance carbon while simultaneously addressing the issue of plastic waste management. This approach supports the development of efficient energy storage systems and promotes environmental sustainability. In addition to energy applications, recent studies have demonstrated the effectiveness of polymer- and biomass-based materials in improving structural, mechanical, and functional performance through hybridization and filler incorporation strategies. Natural fiber-reinforced and waste-derived composites have shown enhanced durability, interfacial bonding, and sustainability potential, supporting the broader concept of converting waste into value-added materials

for advanced applications [47–50]. This idea fits well with the concept of a circular economy, where waste is reused to create new, valuable products[5]. Pyrolysis is one of the most effective methods to convert PET waste into useful hydrocarbons and carbon residues. [6].

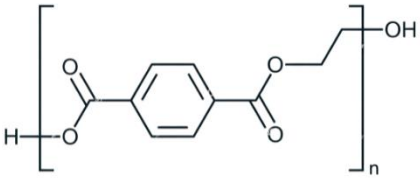

Figure 3. Polyethylene Terephthalate (PET) [7]

EXPERIMENTAL PROCEDURE

Materials and chemicals

Waste Polyethylene Terephthalate (PET) bottles were collected from local shops and hotels. The bottles were first washed with deionized water to remove dust, labels, and residual liquids. After drying, the PET bottles were cut into small square pieces (approximately 1-2 cm). These pieces were used as the main raw material.

Calcium hydroxide ($Ca(OH)_2$) and potassium hydroxide (KOH) shown in Figure4-Figure5 were used as chemical activating agents during pyrolysis. Both chemicals assist in the thermal decomposition of plastic and help in the formation of porous carbon structures by promoting pore development and improving the surface characteristics of the resulting carbon material.

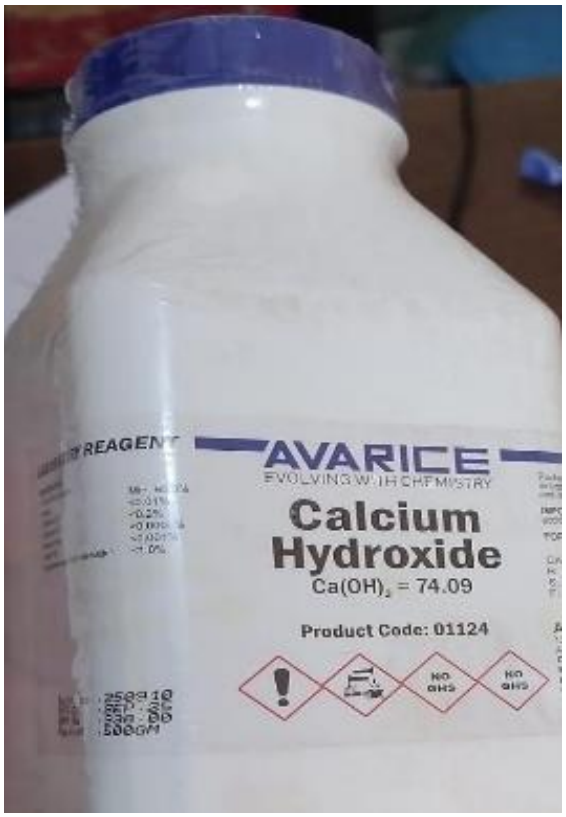

Figure 4. Calcium hydroxide ($Ca(OH)_2$)

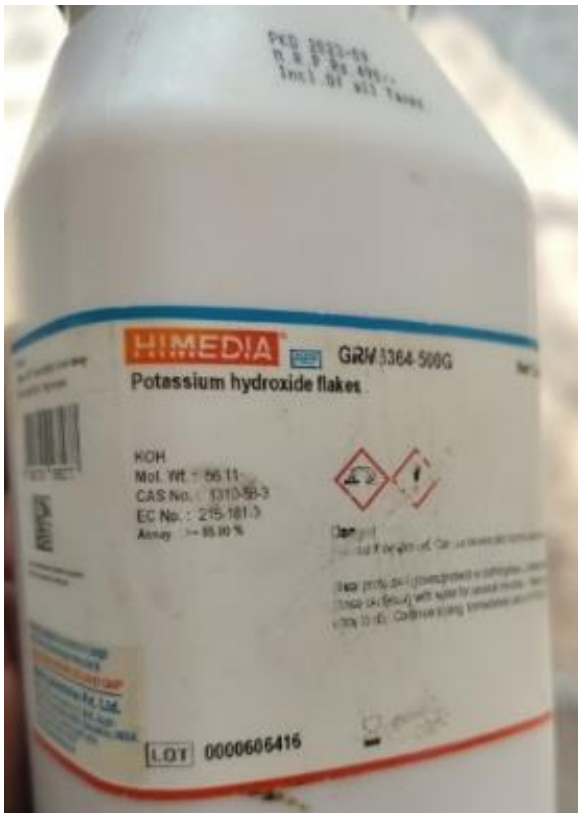

Figure 5. Potassium hydroxide (KOH)

Hydrochloric acid (HCl) shown in Figure6 was used for acid washing to remove residual inorganic impurities after pyrolysis. Distilled water was used for washing and neutralization.

Figure 6. Hydrochloric acid

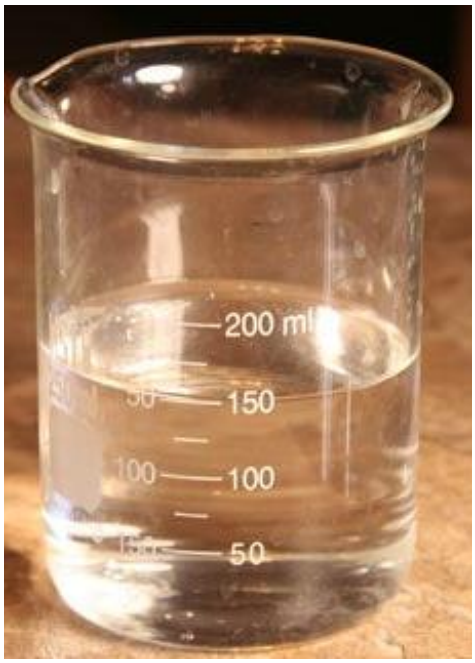

Figure 7. Distilled water

Distilled water - used for washing and neutralization shown in Figure7

For supercapacitor fabrication, carbon black shown in Figure8 was used as a conductive additive to improve the electrical conductivity of the electrode material.

Figure 8. Carbon black

Sodium Carboxy Methyl Cellulose (CMC) and Styrene-Butadiene Rubber (SBR) shown in Figure9-shown in Figure10 were used as binder materials to provide good adhesion and mechanical stability of the electrode.

Figure 9. Carboxy Methyl Cellulose (CMC)

Figure 10. Styrene-Butadiene Rubber (SBR)

Stainless steel mesh (100 mesh size) shown in Figure11 was used as the current collector due to its good conductivity and corrosion resistance.

Figure 11. Stainless Steel (100 Mesh size)

Sodium sulphate (Na_2SO_4) shown in Figure12 aqueous solution was used as the electrolyte for ion transport.

Filter paper shown in Figure13 was used as a separator to prevent short circuit while allowing ionic movement between electrodes.

Equipment Used

The experimental setup included various equipment and instruments used during the synthesis and processing of PET-derived carbon. A hot air oven (100-105 °C) was used for pre-drying PET pieces and for drying after washing. A muffle furnace (750 °C) was employed for the pyrolysis of PET and PET with $Ca(OH)_2$ samples at high temperature. Porcelain crucibles with lids were used to hold the samples during pyrolysis. Glass beakers, funnels, and filter paper were utilized during acid washing, filtration, and neutralization processes, while pH paper was used to monitor the washing stages until neutral pH was achieved. A mortar and pestle were used to grind the dried carbon into fine powder. A magnetic

stirrer or glass rod was used to ensure uniform mixing during acid treatment. Additionally, a digital multimeter was used to measure electrical properties such as voltage, current, and resistance of the synthesized material, helping to evaluate its electrical conductivity and suitability for electrochemical applications.

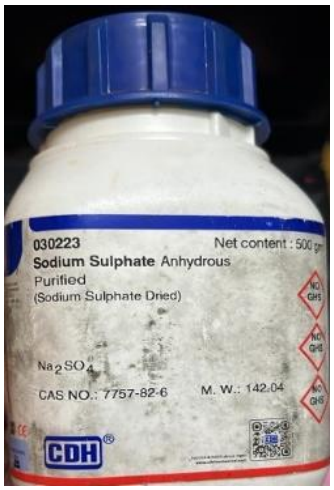

Figure 12. Sodium sulphate (Na_2SO_4)

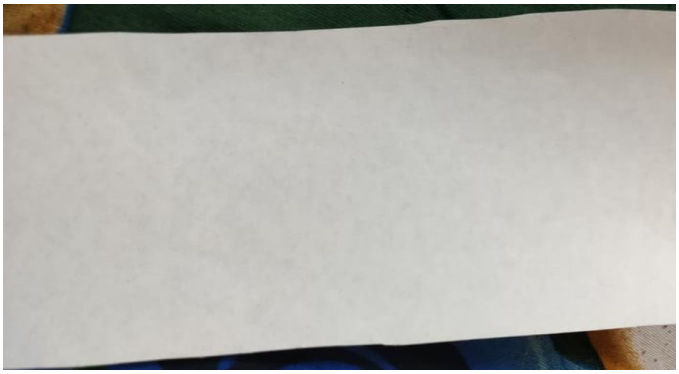

Figure 13. Filter paper

Synthesis of Carbon from Pure PET

The collected PET bottles were first cut into small, uniform pieces (approximately 1-2 cm) to ensure even heat distribution during pyrolysis. These pieces were spread on a tray and dried in a hot air oven at 100-105°C for about 1 hour to remove any moisture, as the presence of moisture can affect the thermal decomposition process. After drying, approximately 50 g of PET pieces were placed into a porcelain crucible, which was tightly covered with a lid to limit the entry of oxygen. This closed environment ensured that the process proceeded under pyrolytic conditions rather than combustion. The crucible was then placed in a muffle furnace, and the temperature was gradually increased at a heating rate of about 5°C per minute up to 700°C. The sample was maintained at this temperature for 2 hours to allow complete thermal decomposition of the PET. During pyrolysis, the PET polymer undergoes thermal degradation, where long polymer chains break down into smaller volatile compounds such as gases and liquid hydrocarbons. Simultaneously, oxygen-containing functional groups are removed, and a carbon-rich solid residue is formed. This residue mainly consists of disordered carbon structures with developing aromatic and graphitic domains. After completion of the heating process, the crucible was removed from the furnace and placed in a desiccator to cool down gradually to room temperature, preventing moisture absorption from the surroundings. The obtained solid product was then collected and ground into a fine powder using a mortar and pestle. This material, shown in Figure14referred to as PET-derived carbon, was used as the reference sample for further study.

Synthesis of Carbon from PET with Chemical activation of $Ca(OH)_2$

To study the effect of chemical activation, approximately 50 g of PET pieces were mixed with an equal amount of calcium hydroxide [$Ca(OH)_2$] powder. The mixing was carried out manually in a beaker to ensure that the PET pieces were uniformly coated with the activating agent. The prepared mixture was then dried in a hot air oven at 100-105°C for about 1 hour to remove moisture. This drying step is important as it improves the interaction between PET and $Ca(OH)_2$ during the thermal process and ensures better activation efficiency. After drying, the mixture was transferred into a covered porcelain crucible to restrict the entry of oxygen and maintain pyrolytic conditions. The crucible was placed in a muffle furnace, and the temperature was gradually increased at a heating rate of approximately 5°C per minute. Initially, the temperature was raised to around 300°C and then further increased to 700°C, where it was maintained for about 2 hour.

Figure 14. Carbon from Pure PET

During pyrolysis, $Ca(OH)_2$ plays an important role in enhancing the decomposition of PET. It promotes the breakdown of polymer chains and facilitates the removal of oxygen-containing functional groups. At high temperatures, $Ca(OH)_2$ can convert into CaO and interact with volatile products, which helps in creating pores within the carbon structure. This results in the formation of a more porous and structurally improved carbon material compared to non-activated PET. After completion of the heating process, the crucible was removed and allowed to cool in a desiccator to avoid moisture absorption. The obtained product, which contained carbon along with calcium-based compounds, was then treated with dilute hydrochloric acid (HCl) to remove residual CaO and $CaCO_3$. The mixture was filtered and washed several times with distilled water until neutral pH was achieved. Finally, the purified carbon was dried in a hot air oven at around 100°C and ground into a fine powder. This material shown in Figure15 was used as $Ca(OH)_2$-activated PET-derived carbon for further characterization and supercapacitor fabrication.

Figure 15. Carbon from PET with $Ca(OH)_2$

Electrode Preparation and Supercapacitor Fabrication

Electrode Preparation

The electrode material was prepared using PET-derived activated carbon as the active material. Carbon black was used as a conductive additive, while sodium carboxymethyl cellulose (CMC) and styrene-butadiene rubber (SBR) were used as binder materials. The composition of the electrode was maintained in the weight percentage of 80:10:5:5 wt%(gm/gm) (active material : carbon black : CMC : SBR). For the preparation of two electrodes, 1.44 g of activated carbon, 0.18 g of carbon black, 0.09 g of CMC, and 0.09 g of SBR were used. Initially, CMC was dispersed in approximately 10-15 mL of distilled water and stirred using a magnetic stirrer until a uniform gel was formed. After complete gel formation, SBR was added and mixed thoroughly to obtain a homogeneous binder solution. Subsequently, PET-derived activated carbon and carbon black were added gradually, and the mixture was stirred continuously until a uniform slurry-like paste was obtained. The prepared slurry was then coated onto a stainless-steel mesh (100 mesh size) current collector. The current collector shown in Figure16 was cut into dimensions of 16 cm × 8 cm, and the slurry was uniformly applied on both sides of the mesh.

This uniform mass loading ensures proper electrochemical performance of the electrode. After coating, the electrodes were dried in a hot air oven at 70°C overnight to remove moisture and ensure strong adhesion of the active material. The dried electrodes shown in Figure17 were then gently pressed to improve contact between the active material and the current collector.

Figure 16. Electrode preparation

Figure 17. Prepared electrodes

Electrolyte Preparation

A 1 M sodium sulfate (Na_2SO_4) aqueous electrolyte was prepared by dissolving 14.204 g of Na_2SO_4 in 100 mL of distilled water. The solution was stirred until complete dissolution was achieved.

Supercapacitor Assembly

For the assembly of the supercapacitor, filter paper was used as a separator. The separator was cut slightly larger than the electrode dimensions and soaked in the prepared electrolyte for approximately 10 minutes to ensure sufficient electrolyte absorption.

The device was assembled in a layered configuration as follows and shown in Figure18-Figure23 [Separator] – [Electrode] – [Separator] – [Electrode] – [Separator]

Figure 18. Separator A

Figure 19. 1st Electrode

Figure 20. Separator B

Figure 21. 2nd Electrode

Figure 22. Separator C

Figure 23. Final product

Since the electrode material was coated on both sides of the current collector, this arrangement ensured effective ion transport and utilization of active material. The assembled structure was then carefully rolled into a cylindrical shape and wrapped with insulating tape to maintain mechanical stability. The cylindrical assembly was placed inside a protective casing and tightly sealed.

RESULT AND DISCUSSION

Fourier Transform Infrared Spectroscopy (FTIR)

Fourier Transform Infrared Spectroscopy (FTIR) is a rapid, non-destructive technique used to identify functional groups in a material by analyzing its absorption of infrared radiation. Different chemical bonds produce characteristic peaks, acting as a fingerprint of the material. It is widely used to determine composition, detect impurities, and study structural changes. For carbon materials, FTIR helps identify oxygen-containing groups and assess the degree of carbonization, which affects electrochemical performance.[8], [9].

FTIR Result Analysis of Pyrolyzed PET

In Figure24 the FTIR spectrum of carbon from pure PET shows characteristic peaks indicating residual functional groups and incomplete carbonization. A broad band at 3200–3600 cm^{-1} represents O–H groups, while a strong peak around 1700 cm^{-1} corresponds to C=O stretching, suggesting remaining ester fragments. Peaks in the 1500–1600 cm^{-1} region indicate aromatic C=C formation, showing partial aromatization. The 1000–1200 cm^{-1} region reflects C–O and C–O–C vibrations, confirming oxygen-containing groups. Weak peaks at 900–600 cm^{-1} indicate aromatic structures. Overall, the results suggest incomplete carbonization with significant oxygen functionalities, which may reduce graphitization and affect electrical and electrochemical performance.[10].

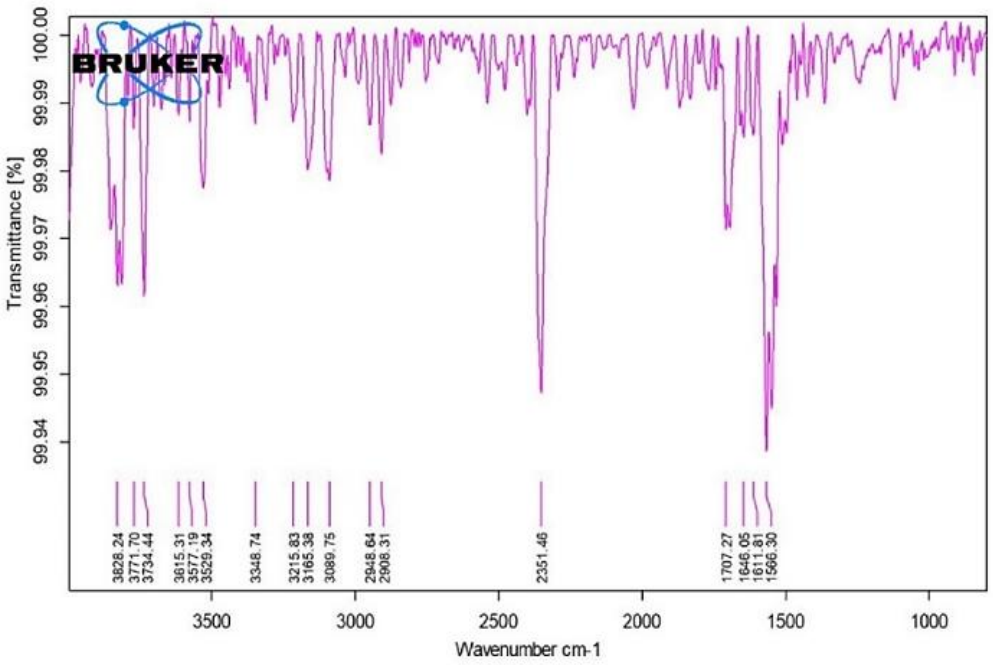

Figure 24. FTIR result carbon from pure PET

FTIR Analysis of Carbon from PET with Ca(OH)₂

In Figure25 the FTIR spectrum of PET-derived carbon activated with $Ca(OH)_2$ shows significant improvement in carbonization compared to pure PET carbon, with a notable reduction or absence of O–H and C=O peaks indicating effective removal of oxygen-containing groups and moisture-related functionalities; a strong peak around 1590–1600 cm^{-1} confirms enhanced formation of aromatic (sp^2) carbon structures, while reduced intensity of C–O peaks suggests fewer residual oxygen functionalities, and peaks at ~880–830 cm^{-1} indicate the presence of stable aromatic frameworks; overall, these results demonstrate that $Ca(OH)_2$ activation enhances PET decomposition, reduces oxygenated groups, and promotes the formation of a more ordered, conductive carbon structure, making it highly suitable for supercapacitor applications due to improved electrochemical performance [11], [12].

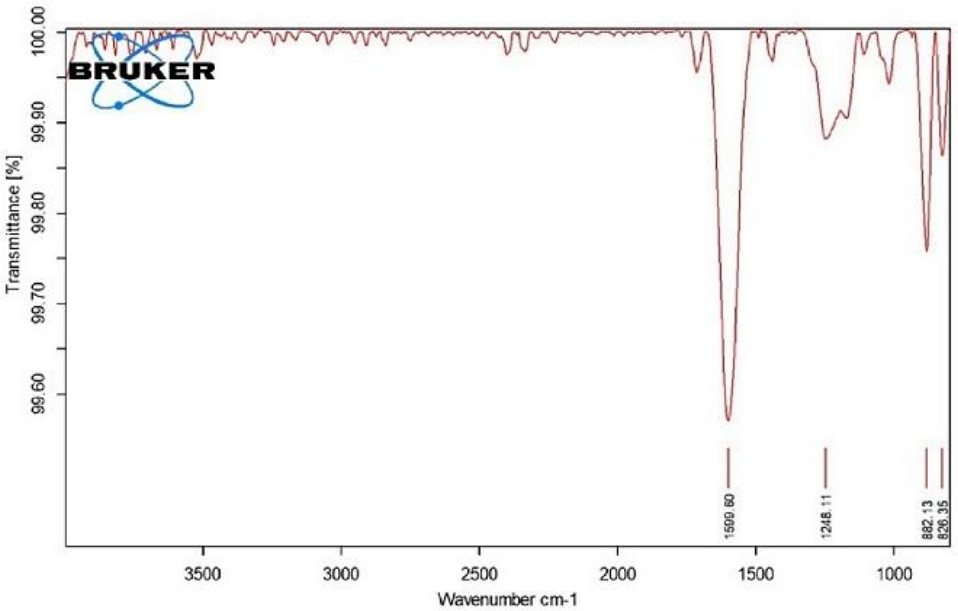

Figure 25. FTIR result carbon from PET with $Ca(OH)_2$

X-Ray Diffraction (XRD)

X-Ray Diffraction (XRD) is a non-destructive technique used to analyze the crystal structure and phase composition of materials. When X-rays (commonly Cu Kα, λ = 1.5406 Å) interact with a sample, they produce diffraction peaks at specific angles following Bragg's Law, which helps determine atomic spacing and structure. Each material has a unique diffraction pattern, allowing phase identification by comparison with standard data. Sharp peaks indicate high crystallinity, while broad peaks suggest small crystallite size or disorder. XRD is widely used to study structure, purity, and crystallinity, especially in nanomaterials and carbon samples.[13-15].

XRD Result Analysis of Pyrolyzed PET

In Figure26 the XRD pattern of carbon obtained from pure PET shows a broad and diffused peak around 2θ ≈ 20°–30°, corresponding to the (002) plane, indicating predominantly amorphous carbon with poor layer stacking and low crystallinity. A weak, broad feature near 2θ ≈ 40°–45° (100 plane) further confirms the absence of well-defined graphitic structure. The lack of sharp peaks suggests high structural disorder and incomplete graphitization, consistent with residual functional groups observed in FTIR. The increased d-spacing compared to graphite (~0.335 nm) indicates defects and irregular layer arrangement. Overall, the material is mainly amorphous with low conductivity, and further activation is needed to improve structural order and electrochemical performance for supercapacitor applications.[16].

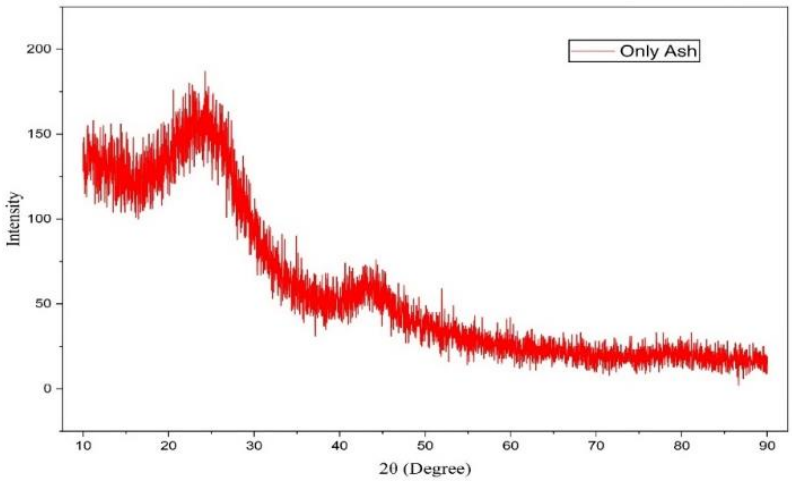

Figure 26. XRD result pyrolyzed PET

XRD Analysis of Carbon from PET with $Ca(OH)_2$

In Figure27 the XRD pattern of PET-derived carbon activated with $Ca(OH)_2$ shows improved structural properties compared to pure PET carbon, with a more defined broad peak at 2θ ≈ 20°–30° corresponding to the (002) plane, indicating better stacking of carbon layers and partial ordering. A slightly clearer peak around 2θ ≈ 40°–45° (100 plane) suggests improved in-plane arrangement of carbon atoms. Although the peaks remain broad, confirming the material is still largely amorphous, the increased peak definition indicates partial graphitization. These improvements are due to the activating role of $Ca(OH)_2$, which enhances PET decomposition, removes volatile components, and promotes the formation of a more organized carbon structure [17].

Scanning Electron Microscopy (SEM)

Scanning Electron Microscopy (SEM) is a high-resolution technique used to study the surface morphology and microstructure of materials using a focused electron beam. It provides detailed images of shape, texture, particle size, porosity, and surface roughness. In carbon materials, SEM is especially useful for analyzing pore structure and surface features, which affect surface area and ion transport, making it important for evaluating materials for supercapacitor applications[18] [19].

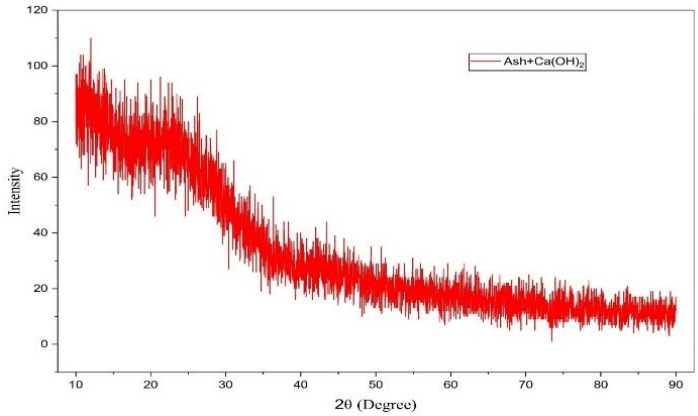

Figure 27. XRD result carbon from PET with $Ca(OH)_2$

SEM Analysis of Carbon from Pure PET

The SEM images **Figure28(a)-Figure28(g)** of carbon derived from pure PET show a dense, irregular, and relatively smooth morphology with limited porosity, consisting of agglomerated particles without a well-developed pore network. Minor cracks and layered features are present but do not significantly enhance porosity, resulting in low surface area and restricted ion transport, which negatively affects supercapacitor performance. The disordered structure also indicates incomplete carbonization, consistent with XRD and FTIR results. Overall, the material exhibits poor porosity and requires chemical activation to improve pore structure and electrochemical performance[20].

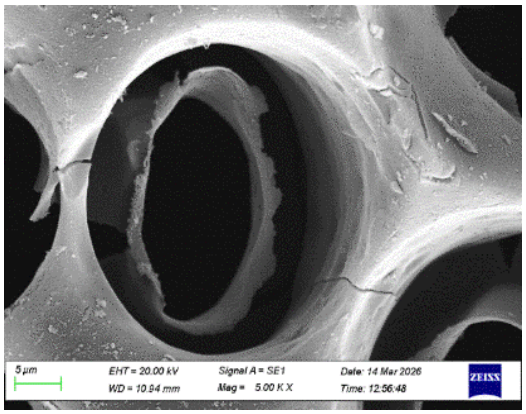

Figure 28. (a) SEM (5 µm)

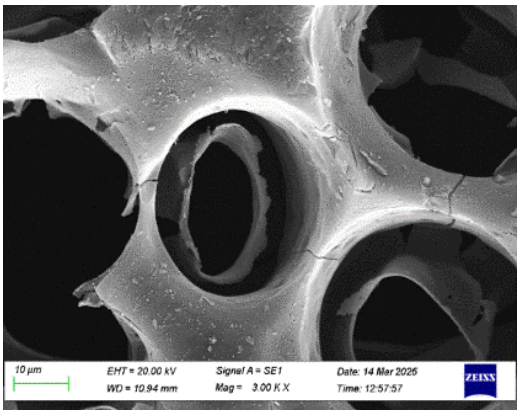

Figure 28. (b). SEM (10 µm)

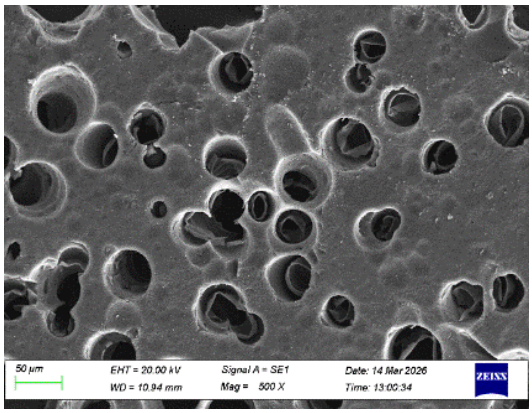

Figure 28. (c). SEM (50 µm)

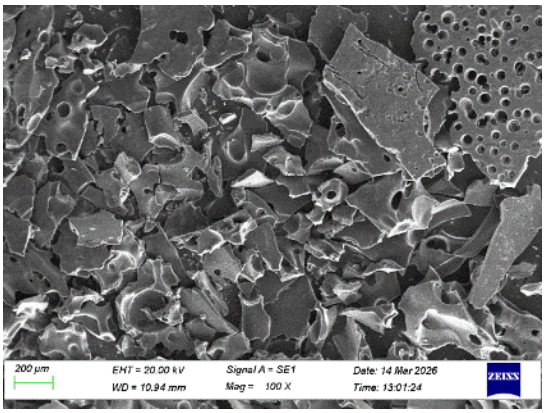

Figure 28. (d). SEM (200 µm

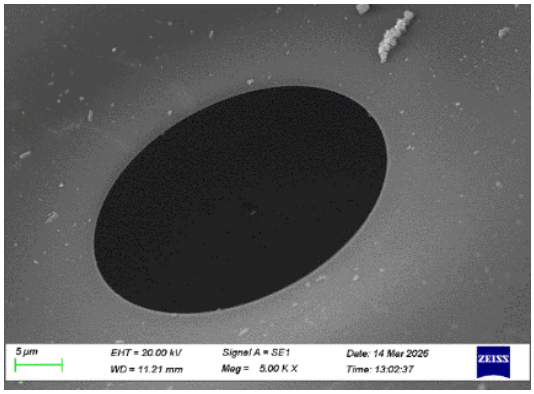

Figure 28. (e) SEM (5 µm)

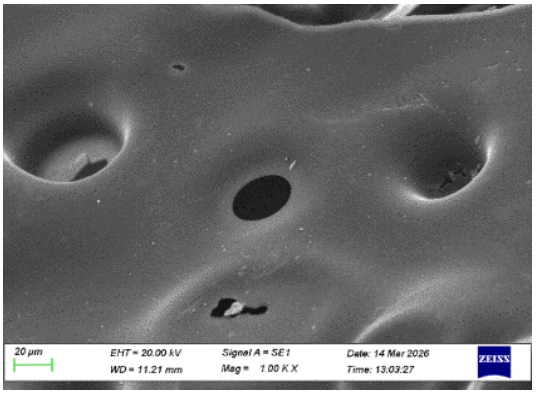

Figure 28. (f). SEM (20 µm)

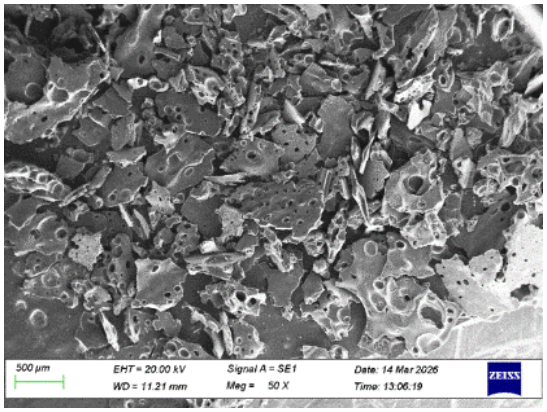

Figure 28. (g). SEM (500 µm)

SEM analysis of carbon from PET with $Ca(OH)_2$

The SEM images of **Figure29(a)-Figure29(g)** PET-derived carbon activated with $Ca(OH)_2$ show a highly rough, irregular, and porous morphology compared to the dense structure of pure PET carbon. The surface exhibits numerous pores, voids, cracks, and interconnected channels, indicating effective breakdown of the polymer matrix during activation. At higher magnification, a well-developed network of micro- and mesopores is visible, formed due to volatile release and the decomposition of $Ca(OH)_2$ during pyrolysis. This porous structure increases surface area, enhances electrolyte accessibility, and improves ion transport. Overall, $Ca(OH)_2$ activation significantly improves the morphology and makes the material more suitable for high-performance supercapacitor applications [21].

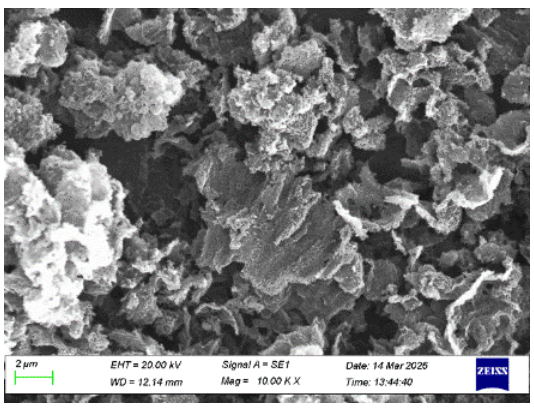

Figure 29. (a). SEM (2 µm)

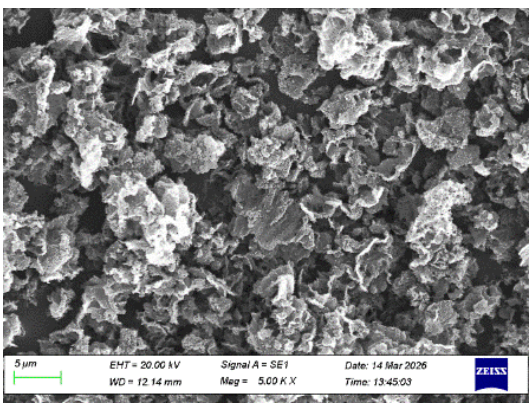

Figure 29. (b). SEM (5 µm)

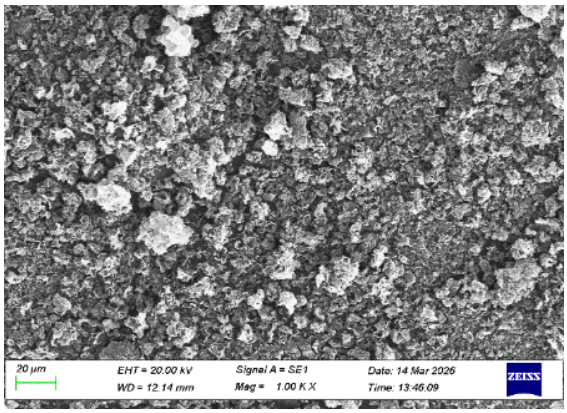

Figure 29. (c). SEM (20 µm)

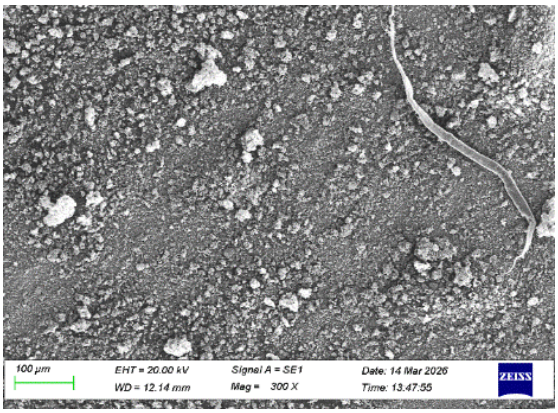

Figure 29. (d). SEM (100 µm)

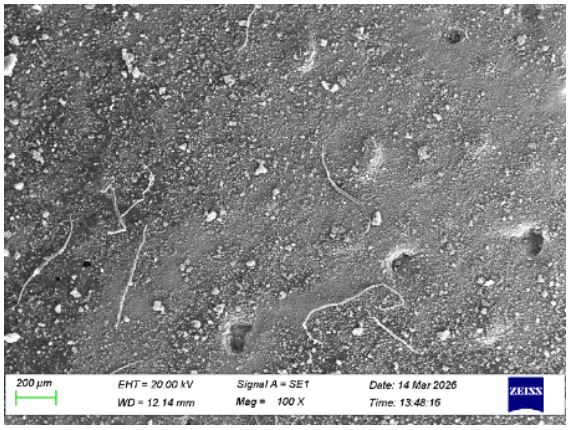

Figure 29. (e). SEM (200 µm)

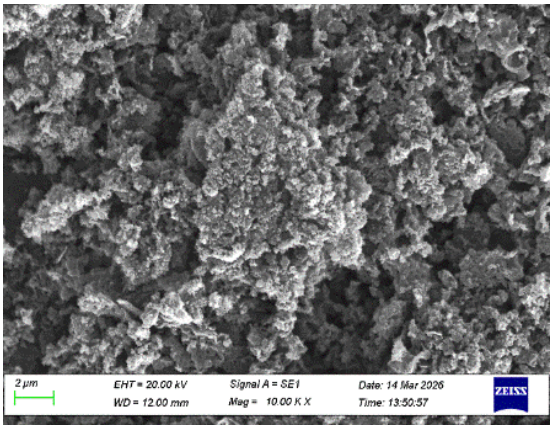

Figure 29. (f). SEM (2 µm)

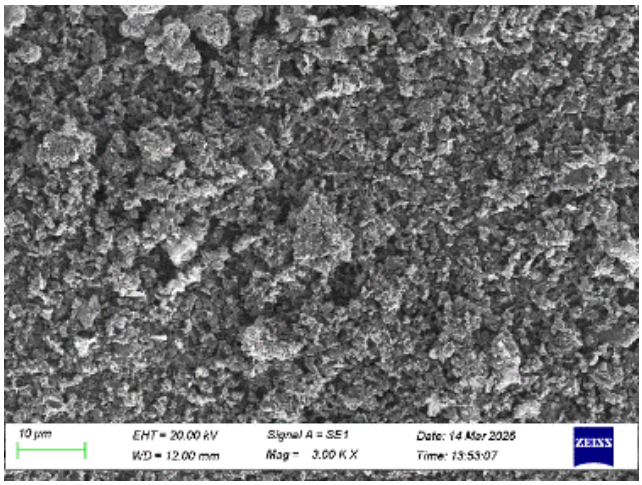

Figure 29. (g). SEM (10 µm)

Transmission Electron Microscopy (TEM)

Transmission Electron Microscopy (TEM) is a high-resolution technique used to study the internal structure and morphology of materials by transmitting electrons through an ultra-thin sample. It provides detailed information about crystal structure, lattice arrangement, defects, and particle size at the nanometer scale. Compared to SEM, TEM offers much higher resolution and is widely used to

analyze structural ordering and crystallinity. In carbon materials, TEM helps identify graphitic layers and pore distribution, which are crucial for electrical conductivity and electrochemical performance in supercapacitor applications[22-24].

Transmission Electron Microscopy (TEM) Analysis of Carbon from Pure PET

TEM analysis of carbon derived from pure PET (**Figure30(a)- Figure30(m)**)shows a heterogeneous and irregular structure consisting of thin sheet-like, rod-shaped, and quasi-spherical nanoparticles forming an agglomerated porous network. The semi-transparent sheets indicate low thickness and amorphous nature, while the absence of clear lattice fringes confirms lack of long-range crystallinity with only limited short-range ordering. SAED patterns display diffuse rings, further indicating predominantly amorphous structure with minor nanocrystalline regions. Overall, this complex nanostructure provides increased surface area and active sites, making the material suitable for supercapacitor applications[25-26].

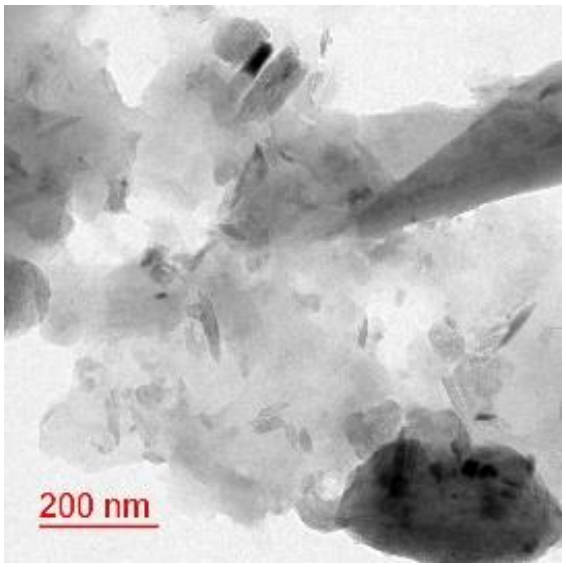

Figure 30. (a) TEM (200 nm)

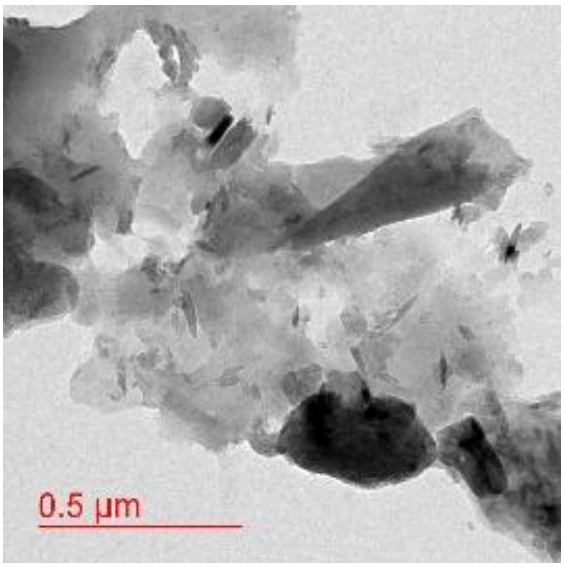

Figure 30. (b) TEM (0.5 µm)

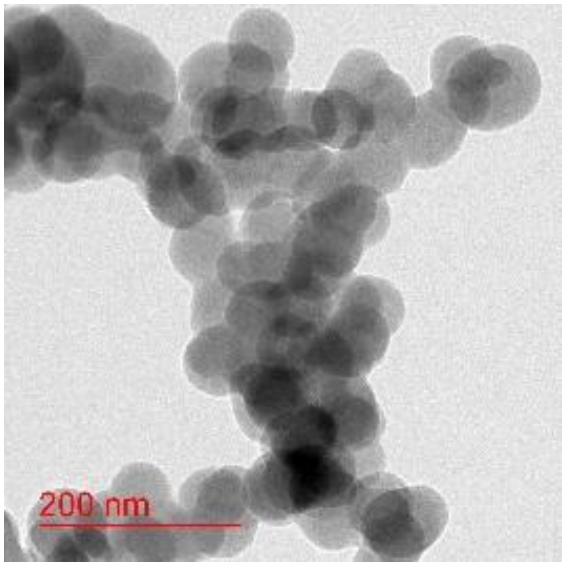

Figure 30. (c) TEM (200 nm)

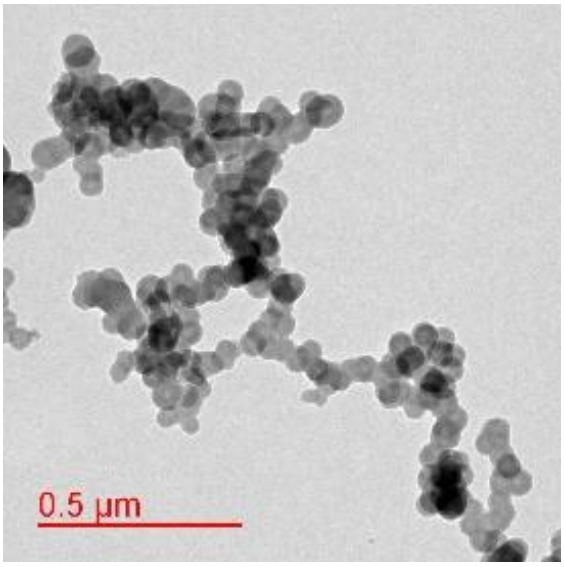

Figure 30. (d) TEM (0.5 µm)

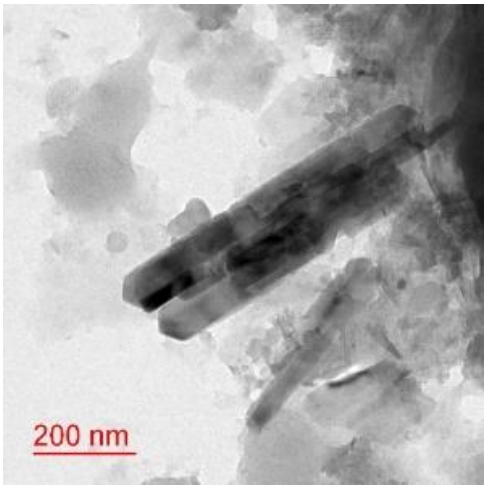

Figure 30. (e) TEM (200 nm)

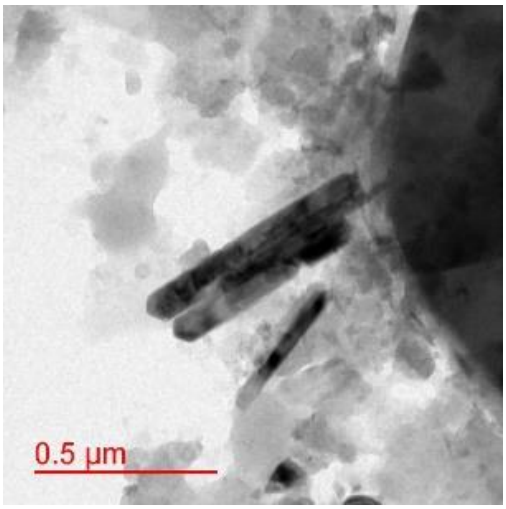

Figure 30. (f) TEM (0.5 µm)

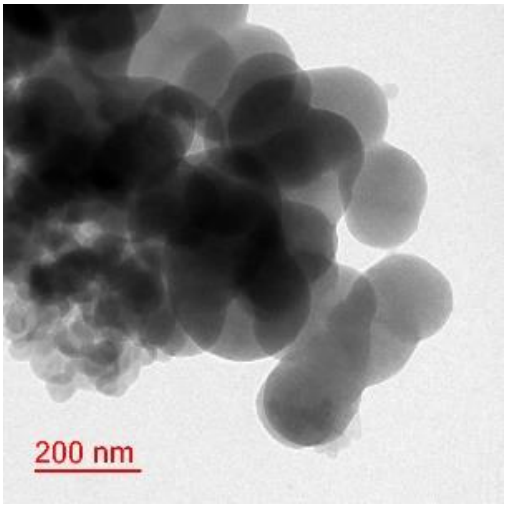

Figure 30. (g) TEM (200 nm)

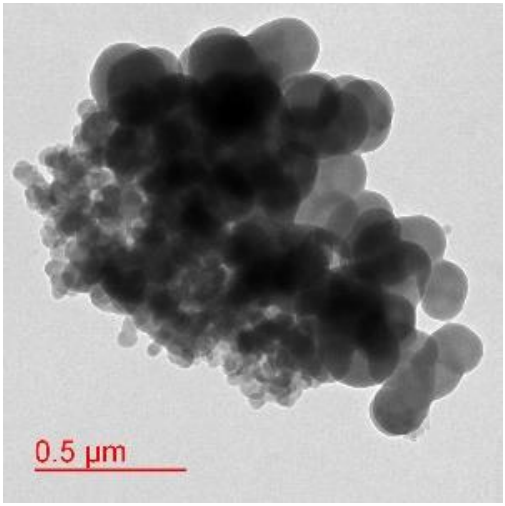

Figure 30. (h) TEM (0.5 µm)

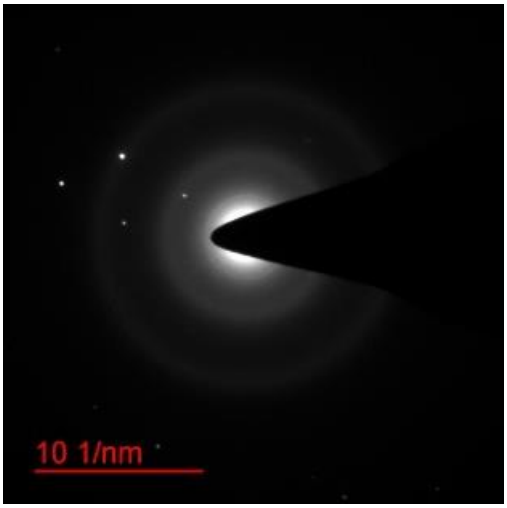

Figure 30. (i) TEM (200 nm)

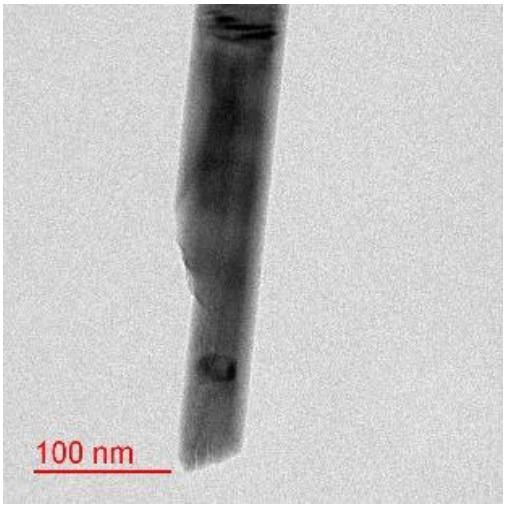

Figure 30. (j) TEM (0.5 µm)

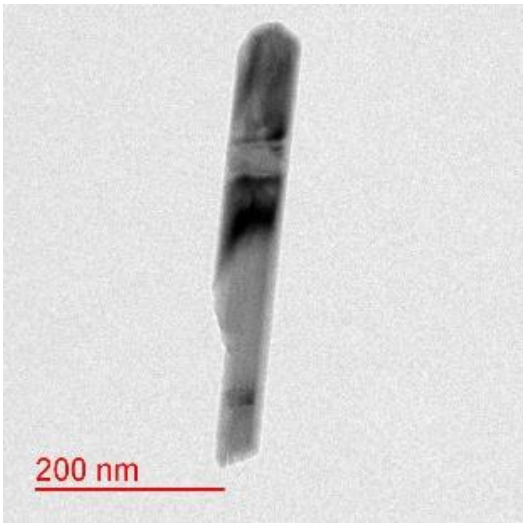

Figure 30. (k) TEM (200 nm)

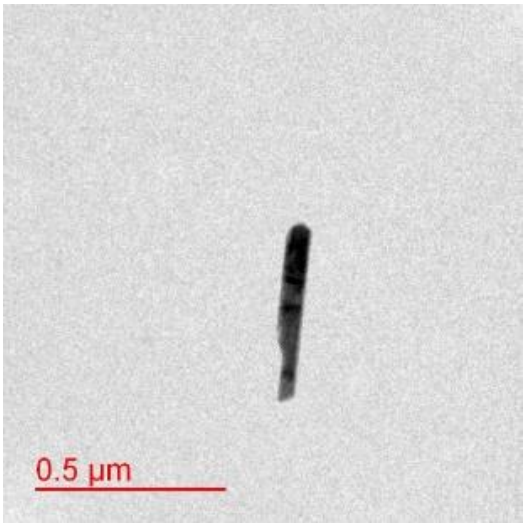

Figure 30. (l) TEM (0.5 µm)

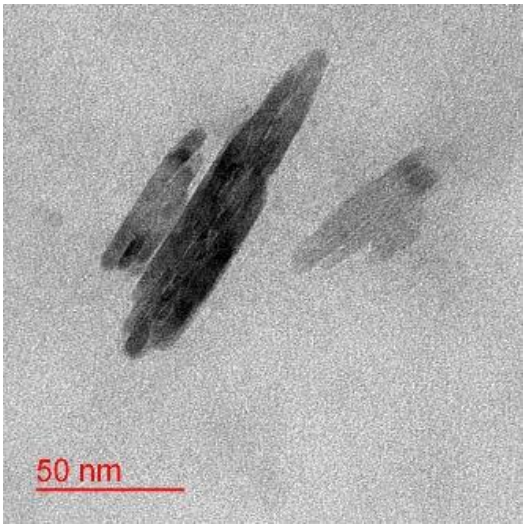

Figure 30. (m) TEM (200 nm)

Transmission Electron Microscopy (TEM) Analysis of Carbon from PET with $Ca(OH)_2$

TEM analysis of PET-derived carbon activated with $Ca(OH)_2$ (**Figure31(a)- Figure31(k))** reveals a highly agglomerated and porous structure composed of irregular nanoscale particles forming sponge-like clusters and a hierarchical pore network. At higher magnifications, interconnected carbon domains with voids and cavities are observed, indicating the formation of meso- and macropores due to PET decomposition and gas evolution during activation. Thin sheet-like or flake structures suggest partial graphitic domain formation, while particle sizes range from ~10–50 nm with larger aggregated structures. Contrast variations indicate heterogeneous density, and SAED patterns show diffuse rings, confirming a predominantly amorphous structure with poor crystallinity. Overall, the material exhibits a porous and complex nanostructure beneficial for electrochemical applications [27].

Raman Spectroscopy

Raman spectroscopy is a technique used to analyze the structural properties of carbon materials by studying their vibrational modes. It identifies graphitization and defects through two main peaks: the D band (~1350 cm^{-1}), representing disorder, and the G band (~1580 cm^{-1}), indicating graphitic (sp^2)

carbon. The intensity ratio (I_D/I_G) reflects the level of defects. It is widely used to evaluate the quality, crystallinity, and structural order of carbon materials for supercapacitor applications[28], [29].

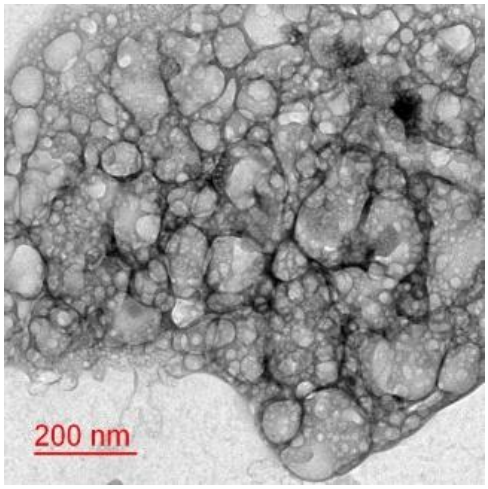

Figure 31. (a) TEM (200 nm)

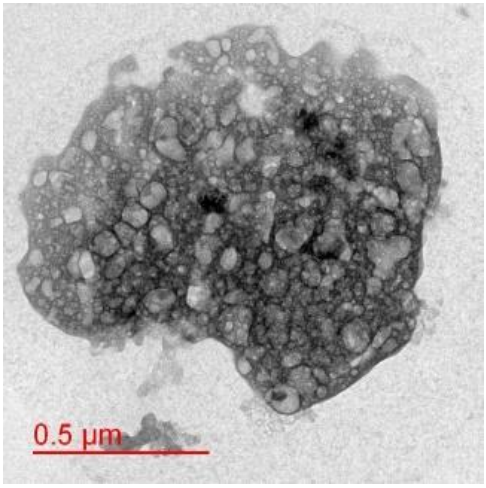

Figure 31. (b) TEM (0.5 nm)

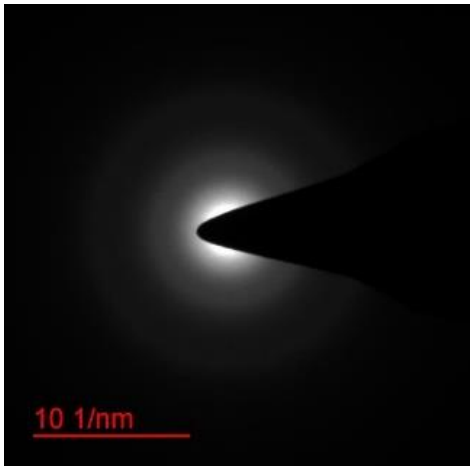

Figure 31. (c) TEM (10.1/nm)

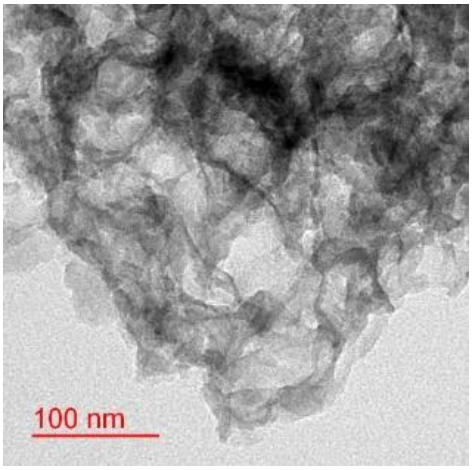

Figure 31. (d) TEM (100 nm)

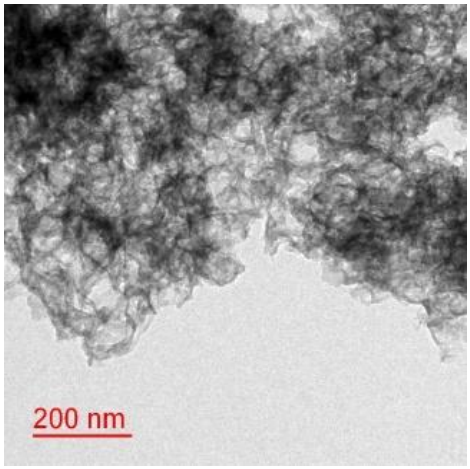

Figure 31. (e) TEM (200 nm)

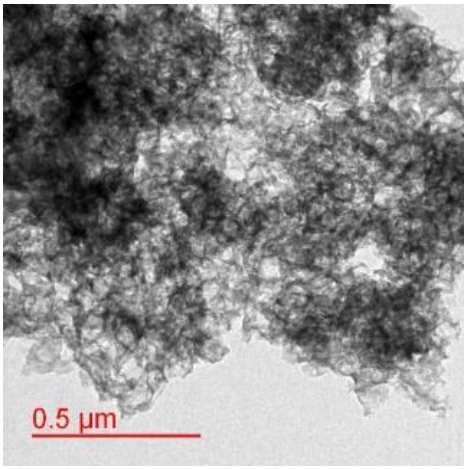

Figure 31. (f) TEM (0.5µm)

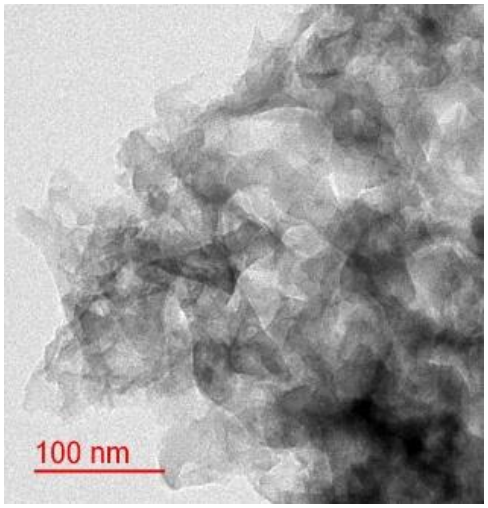

Figure 31. (g) TEM (100 nm)

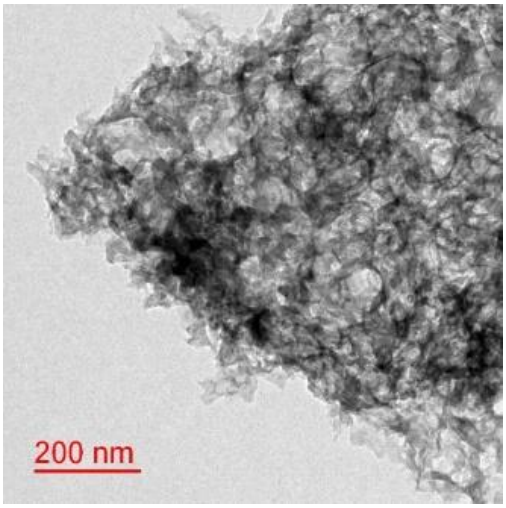

Figure 31. (h) TEM (200 nm)

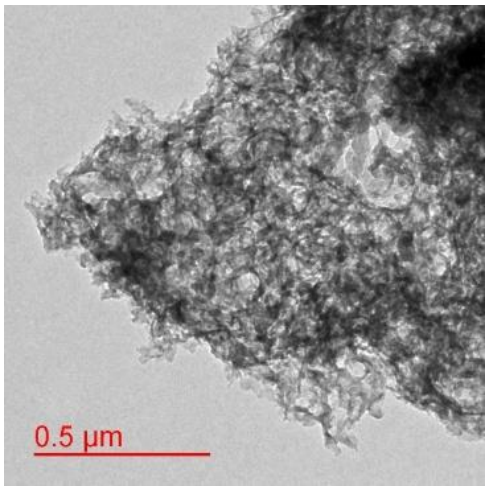

Figure 31. (i) TEM (0.5 µm)

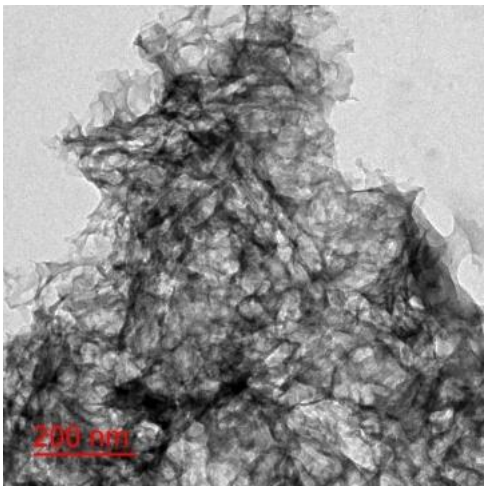

Figure 31. (j) TEM (200 nm)

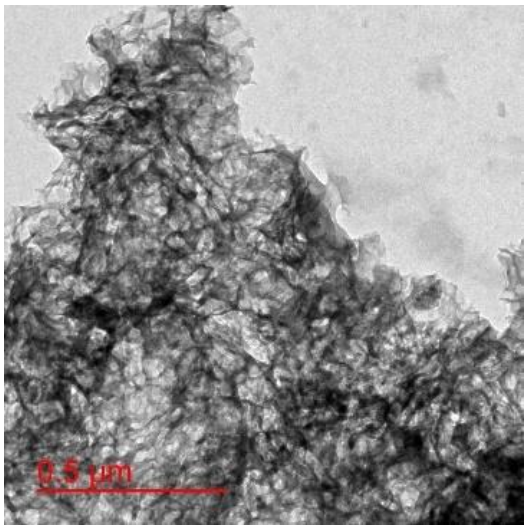

Figure 31. (k) TEM (0.5 µm)

Raman Analysis of Carbon from Pure PET

The Raman spectrum of carbon derived from pyrolyzed PET shown in **Figure32** prominent D (~1330–1360 cm^{-1}) and G (~1580–1600 cm^{-1}) bands, confirming the formation of carbon material with both defects and graphitic domains. The D band indicates structural disorder and edge sites, while the G band represents sp^2 carbon structure. The intensity ratio ($I_D/I_G \approx 0.92$) suggests moderate disorder with coexistence of amorphous and graphitic phases. The weak or absent 2D band further confirms poor graphitic ordering. Overall, the carbon is defect-rich and partially graphitized, providing more active sites and making it suitable for electrochemical applications like supercapacitors[30], [31].

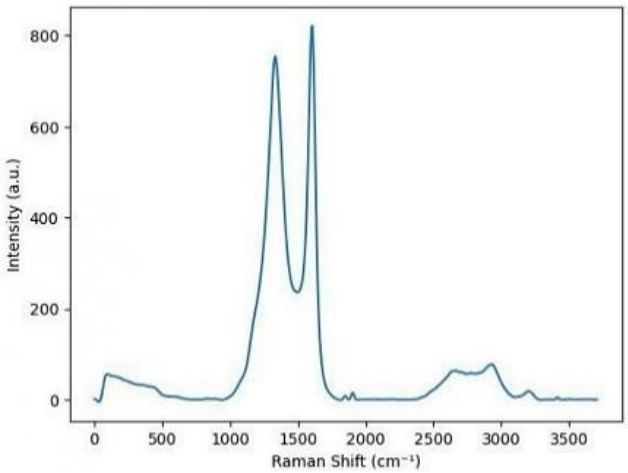

Figure 32. Raman analysis of carbon from pure PET

Raman Analysis of Carbon from PET with Chemical Activation of $Ca(OH)_2$

The Raman spectrum of PET-derived carbon activated with $Ca(OH)_2$ **Figure33** shows prominent D (~1345 cm^{-1}) and G (~1595 cm^{-1}) bands, indicating the presence of both defects and graphitic domains. The increased intensity and sharpness of these peaks compared to pure PET carbon suggest structural modification due to activation. The enhanced D band reflects higher defect density and pore formation, while the clear G band indicates retained sp^2 graphitic structure. Overall, $Ca(OH)_2$ activation introduces defects while maintaining partial graphitization, improving the material's structural properties for electrochemical applications.

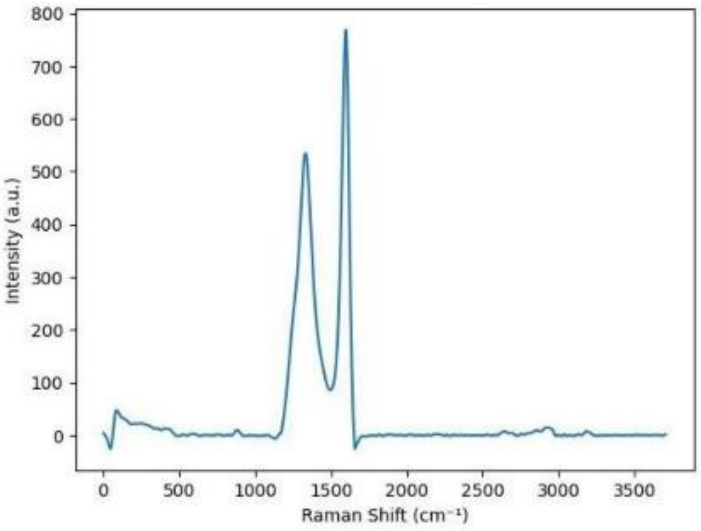

Figure 33. Raman analysis of carbon from PET with $Ca(OH)_2$ activation

Surface Area and Porosity Analysis (BET-BJH Methods)

Brunauer-Emmett-Teller (BET) Analysis

The Brunauer-Emmett-Teller (BET) method is a widely used technique to determine the specific surface area of materials based on gas adsorption. Unlike Langmuir theory, which assumes monolayer adsorption, BET considers multilayer adsorption where gas molecules form successive layers on the surface. The first layer interacts strongly with the solid, while subsequent layers have weaker interactions[32], [33].

Barrett-Joyner-Halenda (BJH) Analysis

The Barrett-Joyner-Halenda (BJH) method is used to determine the **pore size distribution**, **pore volume**, and **average pore diameter** of materials. It is mainly applicable to **mesoporous materials (2–50 nm)**. BJH analysis is based on the concept of **capillary condensation**, which occurs when gas condenses inside the pores at certain pressures. This phenomenon is explained using the **Kelvin equation**, which relates the pore radius to the pressure at which condensation occurs.

Surface Area and Porosity Analysis of Carbon from pure PET (BET-BJH Analysis) BET surface area analysis

The BET analysis of carbon derived from pure PET **Figure34** shows a linear region at $P/P_0 \approx 0.05–0.30$, confirming the validity of the BET model. The material exhibits a high surface area of 725.08 m^2/g and a monolayer adsorption volume of ~166.59 cm^3/g, indicating strong adsorption capacity. Although the BET constant ($C \approx -38.98$) is negative due to surface heterogeneity and microporous nature, the high correlation coefficient (~0.9987) ensures reliable fitting. The total pore volume (0.3812 cm^3/g) and average pore diameter (~1.05 nm) confirm a predominantly microporous structure, making the material suitable for adsorption and electrochemical applications[34], [35].

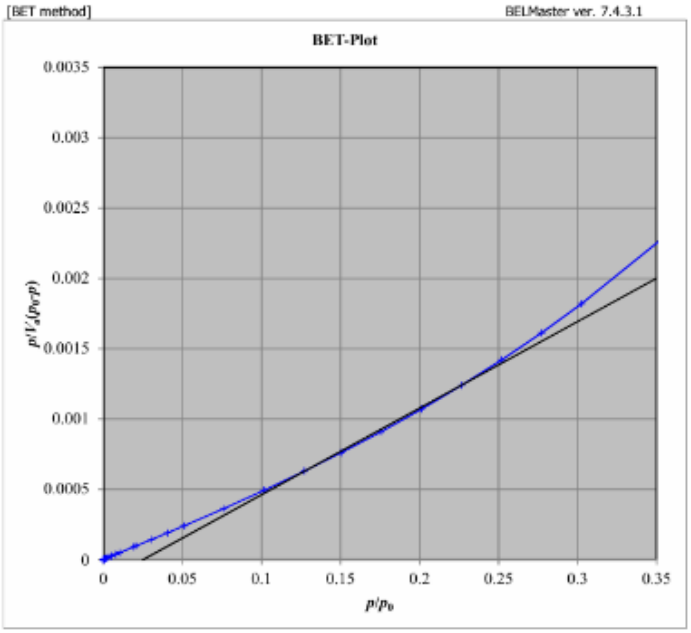

Figure 34. BET surface area plot of carbon from pure PET

BJH Pore Size Distribution

The BJH analysis **Figure35** shows a pore volume of 0.1305 cm^3/g with average, median, and peak pore diameters of ~1.48 nm, 1.30 nm, and ~1.05 nm, respectively, indicating that most pores lie in the 1-2 nm range (microporous to small mesoporous region). Combined BET-BJH results confirm that PET-derived carbon has a high surface area (725.08 m^2/g), high adsorption capacity, predominantly microporous structure (~1 nm), moderate pore volume (0.3812 cm^3/g), and Type I isotherm behavior. These properties make the material highly suitable for adsorption of small molecules like dyes and

pollutants, as well as for supercapacitor applications due to its high surface area, abundant active sites, and efficient ion transport.

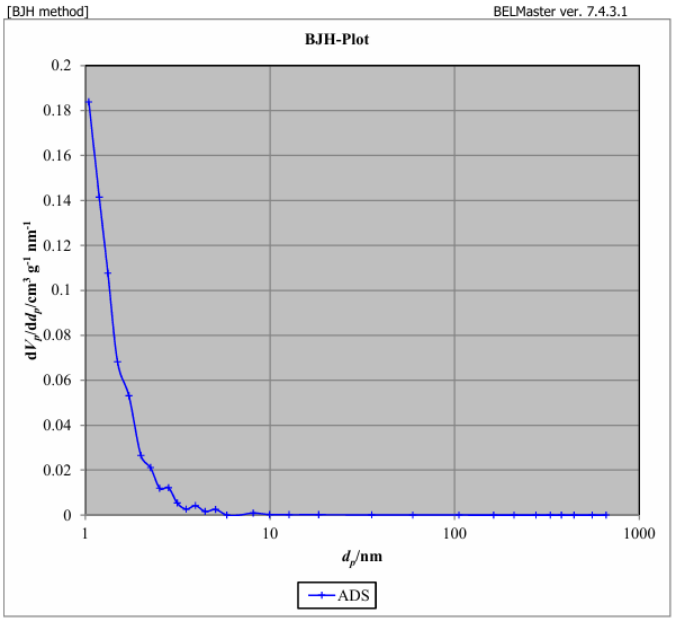

Figure 35. BJH plot of carbon from pure PET

Surface area and porosity analysis of carbon from PET with $Ca(OH)_2$ (BET-BJH analysis) BET surface area analysis

The BET analysis of $Ca(OH)_2$-activated carbon **Figure36** shows a high surface area of 631.37 m^2/g with a monolayer adsorption capacity (V_m) of 145.06 cm^3/g, confirming enhanced pore development due to activation. The BET plot exhibits excellent linearity ($R^2 \approx 0.9996$), indicating reliable results, although the negative BET constant ($C \approx -104.57$) suggests non-ideal adsorption behavior and complex pore structure. The total pore volume (2.1651 cm^3/g) and average pore diameter (~6.86 nm) confirm the presence of mesoporous structures, making the material highly suitable for adsorption and electrochemical applications [36], [37].

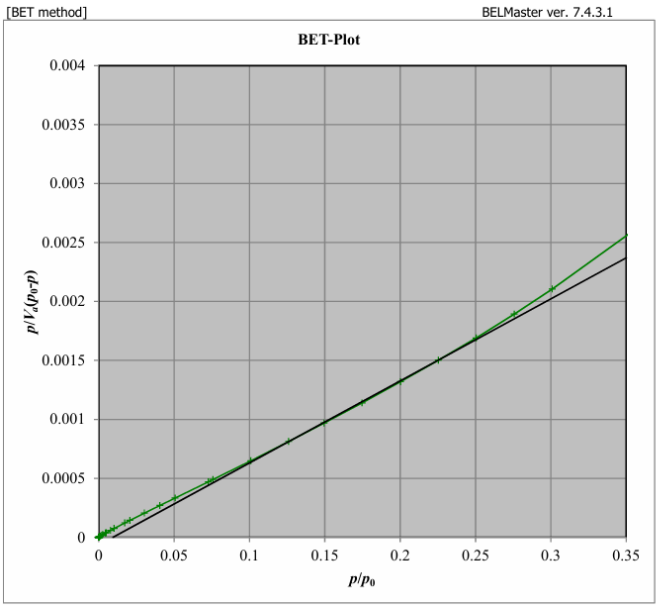

Figure 36. BET surface area plot of carbon from PET with $Ca(OH)_2$

BJH Pore Size Distribution Analysis

The BJH analysis **Figure37** shows a total pore volume of 3.1867 cm^3/g, specific pore surface area of 569.33 m^2/g, and average pore diameter of ~22.39 nm, with median (~80.75 nm) and peak (~1.05 nm) pore sizes indicating a well-developed hierarchical structure. This includes micropores (~1 nm) for charge storage, mesopores (2–50 nm) for ion diffusion, and macropores (>50 nm) for ion buffering. Combined BET–BJH results confirm high surface area (631.37 m^2/g), large pore volume (2.1651–3.1867 cm^3/g), and Type IV isotherm behavior, indicating mesoporosity with micro–meso–macro pore distribution. These features provide abundant active sites, efficient ion transport, and good electrolyte accessibility, making the material highly suitable for high-performance supercapacitor electrodes as well as adsorption and catalytic applications. Similar to observations in polymer and biomass-based composite systems, the overall performance of porous materials is strongly influenced not only by surface area but also by structural organization and accessibility of active sites, where hierarchical structuring plays a key role in enhancing functional efficiency [47–49].

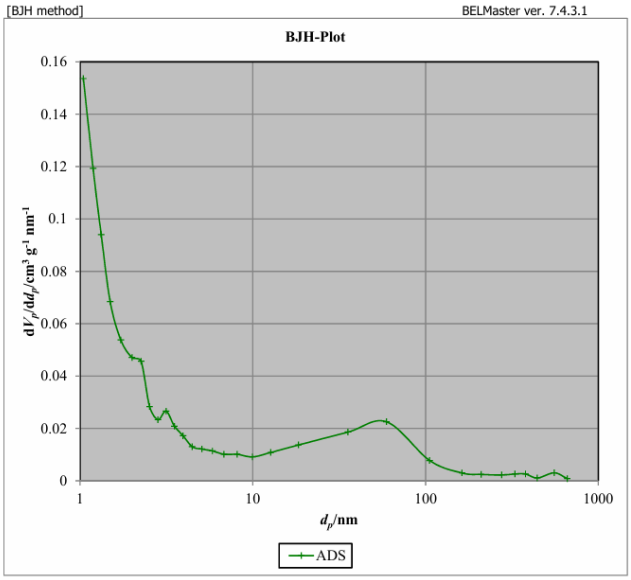

Figure 37. BJH plot of carbon from PET with $Ca(OH)_2$

Comparison with biomass/polymer carbons

Biomass-derived carbons are widely reported to exhibit very high specific surface areas; however, they are often dominated by microporosity, which can limit ion transport and rate capability. In contrast, polymer-derived carbons—particularly those derived from PET—benefit from an intrinsic aromatic backbone that promotes the formation of stable carbon frameworks with partial graphitization.

The $Ca(OH)_2$-activated PET-derived carbon developed in this study exhibits a moderately high surface area (~631 m^2/g) along with a well-defined hierarchical pore structure comprising micro-, meso-, and macropores. Such hierarchical structuring has been widely recognized as a key factor in enhancing functional performance in advanced materials and composite systems [47–50]. Compared to conventional carbons with predominantly microporous structures, this architecture provides improved electrolyte accessibility and ion diffusion pathways.

Therefore, despite having a slightly lower surface area than some highly activated carbons, the present material demonstrates competitive performance due to its optimized pore structure, structural stability, and sustainable synthesis approach.

Improvement in Performance in Terms of Surface Area or Pore Architecture

The results indicate that the improvement in electrochemical performance is governed more by pore architecture than by surface area alone. Although the BET surface area decreases slightly from pure

PET carbon (~725 m^2/g) to $Ca(OH)_2$-activated carbon (~631 m^2/g), the electrochemical behavior improves.

This enhancement is primarily attributed to the development of a hierarchical pore structure:

- Micropores contribute to charge storage,
- Mesopores facilitate ion transport, and
- Macropores act as ion-buffering reservoirs.

Such hierarchical organization improves electrolyte accessibility and ensures efficient utilization of the available surface area. Similar observations have been reported in polymer and hybrid composite systems, where structural organization and internal architecture play a more critical role than bulk material properties alone [47–49]. Therefore, pore architecture is identified as the dominant factor governing performance in the present system.

Fabricated Supercapacitor Performance Analysis

Multimeter Testing and Capacitive Behavior

After fabrication, the supercapacitor showed 0 V initially, which indicates that it was not charged. When it was charged, the voltage increased to about 1.0 V, confirming that the device can store electrical energy. During resistance measurement, it was observed that the resistance value increased gradually with time. This happens because of the charging behavior of the capacitor (RC effect), where current decreases as the capacitor gets charged. In an RC circuit (resistor-capacitor circuit), when a voltage is applied, the capacitor charges gradually and the current decreases with time, which makes the measured resistance appear to increase[38]. Also, ions start accumulating at the electrode-electrolyte interface, forming an electric double layer. This confirms that the device shows proper capacitive behavior [39, 40, 41, 42].

Voltage Retention Behavior

The fabricated supercapacitor was first charged up to approximately 1.0 V, and its voltage was measured over time shown in Figure 38. It was observed that the voltage decreased from 1.0 V to 0.46 V within 10.25 hours, and further reduced to 0.38 V after 19.4 hours. This means the device retained about 38% of its initial voltage, which shows good charge storage ability. The voltage decrease can be understood in three stages. At the beginning, there is a rapid drop due to internal resistance (IR drop). After that, the voltage decreases slowly due to self-discharge and leakage of charge. Finally, the voltage becomes more stable and decreases very slowly. This type of behavior is commonly seen in electrochemical double-layer capacitors (EDLCs), which confirms that the device is working properly[43], [44].

Practical Demonstration using LED

To demonstrate the practical applicability of the fabricated device, three supercapacitors were connected in a series configuration, and a small light-emitting diode (LED) was connected across the terminals shown in Figure 39. It was observed that the LED successfully glowed, indicating that the fabricated supercapacitors are capable of storing and delivering usable electrical energy. The series connection increased the overall output voltage, making it sufficient to power the LED. This practical demonstration confirms the effective energy storage capability of the device, its ability to deliver usable electrical power, and the successful fabrication of a functional supercapacitor. Such demonstrations are commonly employed in laboratory-scale studies to validate the real-world applicability and performance of supercapacitors[45], [46].

The performance achieved in this study demonstrates promising energy storage behavior, especially considering the simple fabrication method and use of low-cost materials. The overall electrochemical characteristics confirm that waste-derived carbon materials can be effectively utilized for sustainable energy storage applications. This behavior is consistent with reports on hybrid composite materials,

where optimized structural design and internal architecture contribute more significantly to performance than individual material properties alone [48–50].

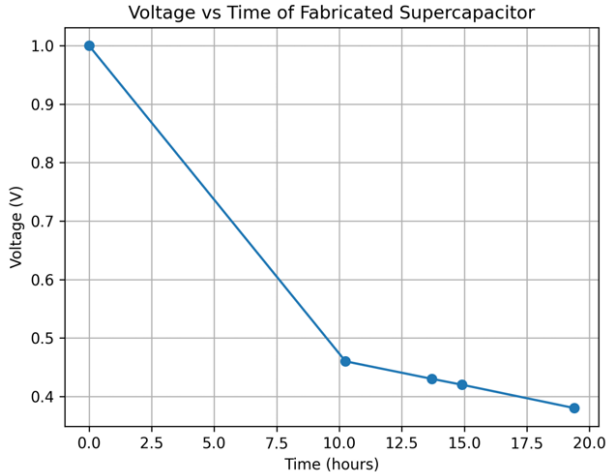

Figure 38. Voltage vs time graph

Figure 39. Practical demonstration using LED

Performance at Different Current Densities

At present, detailed electrochemical measurements such as galvanostatic charge–discharge at varying current densities were not conducted, which we acknowledge as a limitation of the current study. However, based on the structural characteristics of the material, its expected behavior can be reasonably inferred.

At low current densities, the presence of micropores is expected to enable efficient charge accumulation, resulting in higher capacitance. At higher current densities, ion transport limitations typically reduce capacitance in purely microporous materials. However, the hierarchical pore structure observed in the activated carbon—particularly the presence of mesopores—is expected to facilitate faster ion diffusion and improved rate capability.

This behavior is consistent with reports on engineered composite and porous systems, where optimized internal structure enhances transport properties and overall functional performance [48–50]. Therefore, the material is anticipated to exhibit moderate capacitance retention at higher current densities compared to conventional microporous carbons.

Future work will focus on detailed electrochemical characterization, including rate capability analysis, to quantitatively evaluate this behavior.

CONCLUSION

Waste Polyethylene Terephthalate (PET) was successfully converted into porous carbon materials and utilized as an electrode for supercapacitor applications. The combined approach of pyrolysis and chemical activation using $Ca(OH)_2$ proved effective in enhancing the structural and electrochemical properties of the derived carbon. Comprehensive characterization techniques were employed to analyze the material in detail: FTIR confirmed the reduction of oxygen-containing functional groups, indicating improved carbonization; XRD revealed a predominantly amorphous structure with partial graphitization, which was further supported by Raman spectroscopy through the presence of characteristic D and G bands; SEM and TEM analyses showed a transformation from a dense structure in pure PET carbon to a highly porous and interconnected network in the activated carbon, facilitating improved ion transport; and BET-BJH analysis confirmed a high surface area along with a well-developed hierarchical pore structure consisting of micro-, meso-, and macropores, essential for efficient charge storage and electrolyte accessibility. The fabricated supercapacitor device exhibited clear capacitive behavior, stable voltage retention, and effective energy storage capability, while the successful LED demonstration further validated its ability to deliver usable electrical power, confirming its practical applicability. Overall, this work presents a simple, cost-effective, and environmentally sustainable strategy for converting plastic waste into high-performance energy storage materials, highlighting the dual benefit of addressing plastic pollution and developing efficient supercapacitor electrodes, with PET-derived activated carbon showing strong potential for future energy storage applications and contributing to sustainable and circular energy technologies. These findings agree with recent studies on sustainable composite and waste-derived materials, which emphasize the importance of structural tuning, interfacial interactions, and hierarchical design in achieving improved functional performance.

REFERENCE

1. K. Choudhary, K. S. Sangwan, and D. Goyal, “Environment and economic impacts assessment of PET waste recycling with conventional and renewable sources of energy,” in *Procedia CIRP*, Elsevier B.V., 2019, pp. 422-427. doi: 10.1016/j.procir.2019.01.096.
2. F. Alvarado Chacon, M. T. Brouwer, and E. U. Thoden van Velzen, “Effect of recycled content and rPET quality on the properties of PET bottles, part I: Optical and mechanical properties,” *Packaging Technology and Science*, vol. 33, no. 9, pp. 347–357, Sep. 2020, doi: 10.1002/pts.2490.
3. IMPACTS OF PET”.
4. S. Chen and Y. H. Hu, “All-Plastic Supercapacitors from Poly(ethylene terephthalate) Waste,” *Energy and Fuels*, vol. 39, no. 37, pp. 18128–18137, Sep. 2025, doi: 10.1021/acs.energyfuels.5c03370.
5. I. Dědek *et al.*, “Maximizing the electrochemical performance of supercapacitor electrodes from plastic waste,” *J. Energy Storage*, vol. 72, Nov. 2023, doi: 10.1016/j.est.2023.108660.
6. W. Utetiwabo *et al.*, “Electrode materials derived from plastic wastes and other industrial wastes for supercapacitors,” *Chinese Chemical Letters*, vol. 31, no. 6, pp. 1474–1489, Jun. 2020, doi: 10.1016/j.cclet.2020.01.003.
7. G. Balamurugan, I. Mohammed Rafi, and T. Nadu, “An Experimental Study on Plastic Paver Tiles,” *International Journal of Innovative Research in Science, Engineering and Technology (IJIRSET) | Impact Factor: 7.512| ||*, vol. 10, no. 5, p. 4297, 2021, doi: 10.15680/IJIRSET.2021.1005023.

8. Y. Gong, X. Chen, and W. Wu, "Application of fourier transform infrared (FTIR) spectroscopy in sample preparation: Material characterization and mechanism investigation," *Advances in Sample Preparation*, vol. 11, Aug. 2024, doi: 10.1016/j.sampre.2024.100122.
9. A. B. D. Nandiyanto, R. Oktiani, and R. Ragadhita, "How to read and interpret ftir spectroscope of organic material," *Indonesian Journal of Science and Technology*, vol. 4, no. 1, pp. 97–118, 2019, doi: 10.17509/ijost.v4i1.15806.
10. A. Bayu Dani Nandiyanto *et al.*, "FTIR ANALYSIS OF PYROLYSIS OF POLYETHYLENE TEREPHTHALATE (PET) PLASTIC AND ITS PYROLYSIS MECHANISM COMPLETED WITH BIBLIOMETRIC LITERATURE REVIEW FOR SUPPORTING CURRENT ISSUES IN SUSTAINABLE DEVELOPMENT GOALS (SDGS)," 2023.
11. B. Tao *et al.*, "Mechanistic study on the degradation of waste Polyethylene Terephthalate catalyzed by agricultural straw ash," *J. Environ. Chem. Eng.*, vol. 13, no. 6, Dec. 2025, doi: 10.1016/j.jece.2025.120311.
12. M. Efimov, A. Vasilev, D. Muratov, A. Panin, M. Malozovskaya, and G. Karpacheva, "Application of Infrared Pyrolysis and Chemical Post-Activation in the Conversion of Polyethylene Terephthalate Waste into Porous Carbons for Water Purification," *Polymers (Basel).*, vol. 16, no. 7, Apr. 2024, doi: 10.3390/polym16070891.
13. A. Ali, Y. W. Chiang, and R. M. Santos, "X-Ray Diffraction Techniques for Mineral Characterization: A Review for Engineers of the Fundamentals, Applications, and Research Directions," *Minerals*, vol. 12, no. 2, Feb. 2022, doi: 10.3390/min12020205.
14. H. Khan, A. S. Yerramilli, A. D'Oliveira, T. L. Alford, D. C. Boffito, and G. S. Patience, "Experimental methods in chemical engineering: X-ray diffraction spectroscopy—XRD," Jun. 01, 2020, *Wiley-Liss Inc.* doi: 10.1002/cjce.23747.
15. M. Mardani *et al.*, "Phase equilibria in the Fe-Ce-C system at 1100 °C," Jan. 05, 2018, *Elsevier Ltd*. doi: 10.1016/j.jallcom.2017.09.266.
16. Y. Wang *et al.*, "Waste-to-microporous framework: Al/Si fractionation of coal fly ash coupled with waste PET conversion for separated synthesis of high-porosity MIL-53(Al) and ZSM-5 toward efficient dyes and CO2 capture," *J. Mol. Struct.*, vol. 1335, Jul. 2025, doi: 10.1016/j.molstruc.2025.141984.
17. M. Efimov, A. Vasilev, D. Muratov, A. Panin, M. Malozovskaya, and G. Karpacheva, "Application of Infrared Pyrolysis and Chemical Post-Activation in the Conversion of Polyethylene Terephthalate Waste into Porous Carbons for Water Purification," *Polymers (Basel).*, vol. 16, no. 7, Apr. 2024, doi: 10.3390/polym16070891.
18. T. E. Davies, H. Li, S. Bessette, R. Gauvin, G. S. Patience, and N. F. Dummer, "Experimental methods in chemical engineering: Scanning electron microscopy and X-ray ultra-microscopy—SEM and XuM," Nov. 01, 2022, *John Wiley and Sons Inc*. doi: 10.1002/cjce.24405.
19. A. Mohammed and A. Abdullah, "SCANNING ELECTRON MICROSCOPY (SEM): A REVIEW."
20. C. Liu, B. Shi, J. Zhou, and C. Tang, "Quantification and characterization of microporosity by image processing, geometric measurement and statistical methods: Application on SEM images of clay materials," *Appl. Clay Sci.*, vol. 54, no. 1, pp. 97–106, Nov. 2011, doi: 10.1016/j.clay.2011.07.022.
21. E. Moreno, H. A. Murillo, A. Debut, J. R. Mora, and S. Ponce, "High-performance green calcium oxide–biochar catalysts for the chemical recycling of PET waste," *Chemical Engineering Journal*, vol. 530, Feb. 2026, doi: 10.1016/j.cej.2026.173475.
22. M. Ilett *et al.*, "Analysis of complex, beam-sensitive materials by transmission electron microscopy and associated techniques: TEM of Beam Sensitive Materials," Dec. 11, 2020, *Royal Society Publishing*. doi: 10.1098/rsta.2019.0601.
23. S. K. Filippov *et al.*, "Dynamic light scattering and transmission electron microscopy in drug delivery: a roadmap for correct characterization of nanoparticles and interpretation of results," Sep. 26, 2023, *Royal Society of Chemistry*. doi: 10.1039/d3mh00717k.
24. Y. Lin, M. Zhou, X. Tai, H. Li, X. Han, and J. Yu, "Analytical transmission electron microscopy for emerging advanced materials," Jul. 07, 2021, *Cell Press*. doi: 10.1016/j.matt.2021.05.005.

25. G. Jayakumar, A. A. Irudayaraj, and A. D. Raj, "Investigation on the synthesis and photocatalytic activity of activated carbon–cerium oxide (AC–CeO2) nanocomposite," *Appl. Phys. A Mater. Sci. Process.*, vol. 125, no. 11, Nov. 2019, doi: 10.1007/s00339-019-3044-4.
26. A. I. Osman *et al.*, "Production and characterisation of activated carbon and carbon nanotubes from potato peel waste and their application in heavy metal removal.," *Environmental Science and Pollution Research*, vol. 26, no. 36, pp. 37228–37241, Dec. 2019, doi: 10.1007/s11356-019-06594-w.
27. Z. Mirghiasi, F. Bakhtiari, E. Darezereshki, and E. Esmaeilzadeh, "Preparation and characterization of CaO nanoparticles from Ca(OH)2 by direct thermal decomposition method," *Journal of Industrial and Engineering Chemistry*, vol. 20, no. 1, pp. 113–117, Jan. 2014, doi: 10.1016/j.jiec.2013.04.018.
28. S. J. Goldie, S. Bush, J. A. Cumming, and K. S. Coleman, "A Statistical Approach to Raman Analysis of Graphene-Related Materials: Implications for Quality Control," *ACS Appl. Nano Mater.*, vol. 3, no. 11, pp. 11229–11239, Nov. 2020, doi: 10.1021/acsanm.0c02361.
29. D. L. Silva *et al.*, "Raman spectroscopy analysis of number of layers in mass-produced graphene flakes," *Carbon N. Y.*, vol. 161, pp. 181–189, May 2020, doi: 10.1016/j.carbon.2020.01.050.
30. S. Roscher, R. Hoffmann, and O. Ambacher, "Determination of the graphene-graphite ratio of graphene powder by Raman 2D band symmetry analysis," *Analytical Methods*, vol. 11, no. 9, pp. 1180–1191, Mar. 2019, doi: 10.1039/c8ay02619j.
31. S. Sekar and R. Vander Wal, "Upcycling PET plastic waste: A graphenic additive templated approach to synthetic graphite." [Online]. Available: https://ssrn.com/abstract=6168514
32. "BET ANALYSIS".
33. J. Cui *et al.*, "Quantitative Analysis of Virus Adsorption and Co-adsorption Behavior Using BET Modeling and SERS Spectroscopy," *Journal of Physical Chemistry A*, vol. 129, no. 35, pp. 8204–8219, Sep. 2025, doi: 10.1021/acs.jpca.5c03375.
34. A. Kondor, A. Santmarti, A. Mautner, D. Williams, A. Bismarck, and K. Y. Lee, "On the BET Surface Area of Nanocellulose Determined Using Volumetric, Gravimetric and Chromatographic Adsorption Methods," *Frontiers in Chemical Engineering*, vol. 3, 2021, doi: 10.3389/fceng.2021.738995.
35. O. P. Nsude and K. J. Orie, "Microcrystalline Cellulose of Oil Bean Pod: Extraction, Physico-chemical, Brunauer–Emmett–Teller (BET), and Flow-ability Analysis," *Asian Journal of Applied Chemistry Research*, pp. 1–12, Dec. 2022, doi: 10.9734/ajacr/2022/v12i4226.
36. S. Chen and Y. H. Hu, "All-Plastic Supercapacitors from Poly(ethylene terephthalate) Waste," *Energy and Fuels*, vol. 39, no. 37, pp. 18128–18137, Sep. 2025, doi: 10.1021/acs.energyfuels.5c03370.
37. L. Xu *et al.*, "Selective production of terephthalonitrile and benzonitrile via pyrolysis of Polyethylene Terephthalate (PET) with ammonia over Ca(OH)2/Al2O3 catalysts," *Catalysts*, vol. 9, no. 5, May 2019, doi: 10.3390/catal9050436.
38. N. A. Sheikh, D. L. C. Ching, S. Ullah, and I. Khan, "Mathematical and statistical analysis of RL and RC fractional-order circuits," *Fractals*, vol. 28, no. 8, Dec. 2020, doi: 10.1142/S0218348X20400307.
39. B. Babu, P. Simon, and A. Balducci, "Fast Charging Materials for High Power Applications," Aug. 01, 2020, *Wiley-VCH Verlag*. doi: 10.1002/aenm.202001128.
40. R. Yan, M. Antonietti, and M. Oschatz, "Toward the Experimental Understanding of the Energy Storage Mechanism and Ion Dynamics in Ionic Liquid Based Supercapacitors," *Adv. Energy Mater.*, vol. 8, no. 18, Jun. 2018, doi: 10.1002/aenm.201800026.
41. K. Ge, H. Shao, P. L. Taberna, and P. Simon, "Understanding Ion Charging Dynamics in Nanoporous Carbons for Electrochemical Double Layer Capacitor Applications," *ACS Energy Lett.*, vol. 8, no. 6, pp. 2738–2745, Jun. 2023, doi: 10.1021/acsenergylett.3c00369.
42. S. Barcellona, S. Colnago, G. Dotelli, S. Latorrata, and L. Piegari, "Aging effect on the variation of Li-ion battery resistance as function of temperature and state of charge," *J. Energy Storage*, vol. 50, Jun. 2022, doi: 10.1016/j.est.2022.104658.

43. "Voltage Retention Behavior 2".
44. A. Groß and S. Sakong, "Modelling the electric double layer at electrode-electrolyte interfaces."
45. J. J. Quintana, A. Ramos, M. Diaz, and I. Nuez, "Energy efficiency analysis as a function of the working voltages in supercapacitors."
46. A. Bharathi Sankar Ammaiyappan and S. Ramalingam, "Self-Powered Supercapacitor for Low Power Wearable device Applications," Nov. 12, 2021, *IOP Publishing Ltd*. doi: 10.1088/1755-1315/850/1/012016.
47. S. Palanisamy et al., "Wear properties and post-moisture absorption mechanical behavior of kenaf/banana-fiber-reinforced epoxy composites," Fibers, vol. 10, no. 4, p. 32, 2022. doi: 10.3390/fib10040032.
48. K. Aruchamy et al., "Enhancement of mechanical properties of hybrid polymer composites using palmyra palm and coconut sheath fibers: The role of tamarind shell powder," BioResources, vol. 20, no. 1, pp. 698–724, 2024. doi: 10.15376/biores.20.1.698-724.
49. G. Kanat et al., "Utilizing waste manhole covers and fibreboard as reinforcing fillers for thermoplastic composites," Journal of Reinforced Plastics and Composites, 2024. doi: 10.1177/07316844241238507.
50. R. Ramasubbu et al., "Mechanical properties of epoxy composites reinforced with Areca catechu fibers containing silicon carbide," BioResources, vol. 19, no. 2, pp. 2353–2370, 2024. doi: 10.15376/biores.19.2.2353-2370.

